Vortex patterns and energies in a rotating superfluid

L. J. Campbell and Robert M. Ziff*
Los Alamos Scientific Laboratory, Los Alamos, New Mexico 87545
(Received 2 January 1979)

The two-dimensional vortex patterns that occur in a rotating cylinder of superfluid ^{4}He are systematically ordered for numbers of vortices $N = 1, 2, \ldots, 30, 37, 50$ using a prescription for their free energy that is independent of angular velocity and is based upon the justified omission of images. Barrier energies between patterns of the same N and of neighboring N are discussed. A new derivation of the vortex free energy for perfect square and triangular lattices gives the result in terms of $\Gamma(x)$. Patterns that are expected to display high triangular symmetry are studied up to $N = 217$, but circular distortion strongly reduces the region of triangular symmetry even in an unbounded fluid, as shown by the scattering structure factor. According to calculations on arrays containing over one million vortices, the destabilizing velocity at the vortex position R in a finite circular region of a perfect triangular lattice is proportional to $(R/R_0)^5$ where R_0 is the radius of the circular region.

I. INTRODUCTION

The equilibrium state for most fluids in a rotating vessel is rotation of the fluid itself as a solid body. All other possible motions of the fluid eventually decay to this state, driven by dissipative mechanisms which cease once solid-body rotation is attained. An exception to this rule is shown by the superfluid phase of liquid ^{4}He. According to the two-fluid hydrodynamics which it obeys, the so-called normal component may rotate but the superfluid component cannot (it is curl free).[1] The superfluid may, however, form singular vortex lines with circulations quantized in units of $\kappa = h/m \approx 0.001$ cm^2/sec, where h is Planck's constant and m is the mass of the ^{4}He atom. The equilibrium, dissipationless state of the superfluid component in a cylinder rotating parallel to its axis consists of an array of such vortices, each of which is parallel to the axis of rotation and has one unit of circulation. The array itself is in solid-body rotation. For sufficiently fast rotation rates this vortex array is dense and nearly uniform and effectively simulates solid-body rotation of the fluid on a distance scale large compared to the spacing of the vortices. However, for very slow rotation rates there may be just a few vortices, or even none, and the relative difference between successive equilibrium states is large and observable. In this paper we will examine some of the properties of these low-lying vortex states.

Studies of vortex lines, and even of arrays of vortex lines, were undertaken long before superfluidity in helium was known to exist. The motion and stability of rings of several vortex lines were considered by Lord Kelvin, J. J. Thompson, and T. H. Havelock,[2] all more than a half century ago. The problem of determining the rotational equilibrium states of an irrotational fluid was studied much more recently, motivated by the superfluidity of helium. This problem amounts to finding the number and configuration of quantized vortices which globally minimize a free-energy function $F = E - \Omega L$, where E is the total kinetic energy in the superfluid motion, L is its angular momentum, and Ω is the rotational speed of the bucket.[1] Hess[3] calculated F explicitly for a single ring of vortex lines in a cylindrical container and also for a ring with one vortex in the center, and found the equilibrium number and configuration for $N = 0$ through 8 as a function of Ω. Stauffer and Fetter[4] were the first to report computer calculations of vortex patterns and published pictures of two different patterns of 37 vortices and their free energies for one value of Ω.

Now, after some years of work by themselves and by others, Gordon, Williams, and Packard[5] have presented photographs of patterns of vortices in superfluid helium. Motivated in part by this work we have made a systematic numerical study of stationary vortex patterns and their free energies for $N = 1$ to 30, and also for certain N up to 217. In Sec. II we discuss the theory and the procedure we used and in Sec. III we discuss the results for single patterns. In Sec. IV, we discuss the barriers in free energy between patterns. We close with a summary of our conclusions and some final remarks. Appendices A and B contain, respectively, derivations of a sum rule due to Kirchhoff and of the free energy of the continuum model (for both square and triangular versions). The destabilizing velocity in large, triangular arrays is discussed in Appendix C.

II. DETERMINATION OF STABLE VORTEX PATTERNS

The free energy per unit lenth of a system of N rectilinear vortices in a rotating cylindrical vessel is given by[6]

$$f = -\sum_{j>i=1}^{N} \ln(r_i^2 + r_j^2 - 2r_i r_j \cos\theta_{ij}) + \frac{1}{2}\sum_{i,j=1}^{N} \ln(1 + r_i^2 r_j^2 - 2r_i r_j \cos\theta_{ij}) - \omega \sum_{i=1}^{N} (1 - r_i^2) + N \ln(R/a) \quad . \tag{1}$$

In the reduced units $f = (4\pi/\rho\kappa^2)F$ and $\omega = (2\pi R^2/\kappa)\,\Omega$. Here ρ is the density of the superfluid, R is the radius of the bucket, a is the vortex core radius, r_i is the radial distance to the ith vortex from the axis of the cylinder in units of R (so that in these units the radius of the bucket is unity), and $\theta_{ij} = \theta_i - \theta_j$ is the angle between r_i and r_j. This function f must be minimized for all N and r_i to find the stable pattern for a given ω. This procedure can be carried out analytically for only small numbers of vortices, perhaps $N < 9$, corresponding to the equilibrium states for small values of ω. Numerically, a stable pattern of any number N can be found by the following iterative scheme: Begin with an arbitrary pattern of vortices and assign to each vortex a vector equal to the negative gradient of the free energy with respect to its coordinates: $\vec{u}_i = -\frac{1}{2}\vec{\nabla}_i f$. Move each vortex a step proportional to $\vec{u}_i$, then calculate the new values of $\vec{u}_i$ and repeat. Each iteration produces a pattern of lower free energy if the constant multiplying each $\vec{u}_i$ is sufficiently small. Eventually, the positions converge (as all $\vec{u}_i$ approach zero) to a pattern which minimizes f, at least with respect to small displacements of the vortex positions.

From Eq. (1) we can calculate $\vec{u}_i$. It is convenient to introduce complex notation $z_j = r_j \exp(i\theta_j)$, $\bar{z}_j = \text{conjugate}(z_j)$ which allows Eq. (1) to be written

$$f = -\sum_{i<j} \ln|z_i - z_j|^2 + \frac{1}{2}\sum_{i,j} \ln|1 - z_i \bar{z}_j|^2 - \omega \sum_i (1 - |z_i|^2) + N \ln(R/a) \quad . \tag{2}$$

The relation $\vec{u}_k = -\frac{1}{2}\vec{\nabla}_k f$ becomes, in complex notation, $u_k = \partial f/\partial \bar{z}$, where $u_k = u_{k,x} + i u_{k,y}$. Using Eq. (2) we find

$$u_k = \sum_j{}' \frac{1}{\bar{z}_k - \bar{z}_j} - \sum_j \frac{1}{\bar{z}_k - 1/z_j} - \omega z_k \quad , \tag{3}$$

where the prime on the first summation indicates that $j \neq k$. That summation represents the direct contribution of all the other vortices and the second summation represents the contribution of the image vortices. For each vortex at (r_i, θ_i), the image vortex is at $(1/r_i, \theta_i)$ and has opposite circulation. In complex notation, the image of a vortex at z_i is at $1/\bar{z}_i$.

It turns out that each of these vectors u_k is orthogonal to the classical (dimensionless) hydrodynamic velocity of motion v_k of the same vortex in the rotating frame of reference, $v_k = iu_k$. When f is at a minimum both these velocities are zero at every vortex, and so the positions of the vortices of a stable pattern are stationary in the rotating frame of reference. Note that the iterative displacements toward an equilibrium pattern in the direction u_k are not identical to the physical approach to equilibrium, which depends upon the dissipative mechanisms. In the complete absence of dissipation the free energy is never changed by the hydrodynamic motion v_k of the vortices since the v_k are directed along the equipotentials of f. Due to the dissipation caused by the interaction of the vortices with the normal fluid, which seeks solid-body rotation, the actual motion of the vortices will always be some combination of u_k and v_k. The displacements we use here, purely in the direction of u_k, are a computational method of finding stable patterns in the quickest way. Presumably, all patterns found this way are physically accessible by the actual vortex motion.

We employed the iterative procedure described above, using the u_k given by Eq. (3), to search for stable patterns. For the initial configurations, we used either random arrays or certain symmetrical patterns (vortices arranged in concentric circles). In these computations we found that the patterns have the following general properties (several of which were also reported by Stauffer and Fetter[4]):

(i) For a given rotation speed ω, there are many patterns, with various numbers of vortices N, that are locally stable (except for very low values of ω at which there might be just one or even no stable pattern). The pattern that has the lowest f is the absolutely stable one and, thus, is the equilibrium pattern for that ω.

(ii) For each value of N, there are usually (always, for $N \geq 9$) multiple configurations, which differ among themselves only slightly in free energy. As ω varies, the configurations change in size, but remain qualitatively distinct, i.e., there is no shifting between two patterns of the same N. The relative ordering in free energy among these different patterns of the same N always remains the same. Thus, we can designate these patterns by N, subscripted by $1, 2, 3, \ldots$, in order of increasing free energy.

(iii) The positions of the vortices fall very closely, or exactly when symmetry allows, into concentric rings. This is a result of the circular symmetry of the boundary, as well as the symmetry of the rotation itself. We show later that this circular symmetry persists in the absence of the boundary.

(iv) As ω is lowered, the patterns enlarge toward the boundary, and remain stable only above a certain value ω^*. This value depends upon N and also upon the particular configuration. We found that $\omega^* \approx N + c$, where c is of order 1 for $N = 1$ to 20. For a simple ring of vortices in a cylindrical vessel, $N = 1$ to 6, Havelock[2] calculated these ω^*, and with care we were able to find the same values to about three digits of accuracy, at best.

Clearly, the task of finding all the stable patterns and calculating their free energies for many values of N and wide ranges of ω would be tedious, and the results of such a program would produce too much data to conveniently communicate or even use. However, a significant simplification occurs if the images are completely left out of the calculations. We found this is permissible because their contribution is sufficiently small. Without images, the calculations themselves are easier, but more importantly, the calculations need be done for only one value of ω for each pattern because the results can be easily scaled.

First of all, the expression for the iteration vectors is simplified to

$$u_k = \sum_j{}' \frac{1}{\bar{z}_k - \bar{z}_j} - \omega z_k \quad , \tag{4}$$

because the second summation of Eq. (3) represents the contribution of the images. This implies that the radii of the vortices in a given pattern change with ω according to the simple relation $r_i^2 \omega = \text{const}$, because Eq. (4) scales this way when $u_k = 0$ (local equilibrium). Using this relation a stable pattern found for a single value of ω can be scaled to any ω.

Secondly, the contribution of the images to the free energy, the second summation in Eqs. (1) and (2), may be dropped. Also, omitting images makes the angular-momentum term in f trivial when $u_k = 0$ (i.e., when the array rotates as a solid body)

$$-\omega \sum_{j=1}^{N} (1 - r_j^2) = -\omega N + \tfrac{1}{2}[N(N-1)] \quad . \tag{5}$$

Equation (5) shows that different stationary patterns, both stable and unstable, with the same N and ω have exactly the same angular momentum.[7] We give a simple derivation of Eq. (5) in Appendix A. It is a consequence of a general integral of vortex motion due to Kirchhoff.[8]

Thirdly, we may write the first summation in Eq. (2)

$$-\sum_{i<j} \ln|z_i - z_j|^2 = \frac{N(N-1)}{2} \ln\omega - \sum_{i<j} \ln\omega |z_i - z_j|^2 \quad . \tag{6}$$

The last term above is independent of ω, since ωr_i^2 is constant, and the entire ω dependence is displayed in the first term. Thus, by omitting images and using Eqs. (5) and (6) the free energy becomes,

$$f_0 = -\sum_{i<j} \ln\omega |z_i - z_j|^2 + \frac{N(N-1)}{2} \ln\omega - \omega N + \frac{N(N-1)}{2} + N \ln\left[\frac{R}{a}\right] \quad . \tag{7}$$

The subscript 0 indicates that images are omitted. This expression is valid only for a stationary configuration because we used Eq. (5).

If the double summation above is approximated by an integral plus a correction term that accounts for the discrete nature of the vortices, then Eq. (7) becomes

$$f_c(N, \omega) = \frac{3N^2}{4} - \frac{N^2}{2} \ln N - \omega N + \frac{N(N-1)}{2} \ln\omega - Nb + N \ln(R/a) \quad , \tag{8}$$

where

$$b = \ln[\Gamma(\tfrac{1}{3}) 3^{1/2} (2\pi)^{-3/2}] = 0.748\,752\,485$$

for a triangular array as shown in Appendix B. This result is equivalent to the so-called continuum model discussed by Stauffer and Fetter,[4] and we denote it by the subscript c. Because the continuum model approximates the actual free energy very closely it will be quite useful in analyzing the stable vortex patterns. In particular, the difference between f_0 and f_c provides a distinguishing energy label, which is independent of ω,

$$\Delta f_0 \equiv f_0(N, \omega) - f_c(N, \omega) = -\sum_{i<j} \ln\omega |z_i - z_j|^2 - \frac{N^2}{4} + \frac{N^2}{2} \ln N + N(b - \tfrac{1}{2}) \quad . \tag{9}$$

Because Δf_0 is always small (of order unity) and constant, we will use it to specify the free energy. We can also define the difference $\Delta f = f - f_c$. Because image effects vanish in the limit of large ω and fixed N we have $\lim_{\omega\to\infty} \Delta f = \Delta f_0$.

In Table I we list, as an example, the values of free energy for the pattern 18_1 (the pattern of 18 vortices with the lowest free energy). For each ω we calculated the positions of the vortices using Eq. (3), which takes into account the images, and then calculated the free energy $f - N \ln(R/a)$ according to Eq. (2) (we are not interested here in the dependence upon R/a). For comparison, we calculated the positions and free energies *without* images using Eqs. (4) and (7). The difference $f - f_0$ is listed in the third column of Table I. It is quite small except for ω near ω^*, which is about 19.9 for this pattern. For pattern 18_1 we find $\Delta f_0 = 0.252\,41$. We also show the pro-

TABLE I. As a function of the dimensionless angular velocity ω, the dimensionless free energy f for vortex pattern 18_1 is listed and compared with the corresponding free energy f_0 calculated without images. The fourth column shows the variation of the radius of the outermost vortex in this pattern.

ω	$f-N\ln(R/a)$	$f-f_0$	$\omega^{1/2}r$
90	−1169.994 48	0.000 00	3.515 859
80	−1008.015 30	0.000 01	3.515 868
70	−848.445 60	0.000 01	3.515 890
60	−692.030 67	0.000 03	3.515 943
50	−539.925 93	0.000 09	3.516 094
40	−394.067 10	0.000 30	3.516 637
30	−258.083 89	0.001 73	3.519 597
25	−195.984 38	0.007 02	3.527 177
20	−140.181 33	0.063 01	3.612 616

duct $\omega^{1/2}r$, where r is the radius of the vortex that is the farthest from the center. The variation is very small except for ω near ω^*, and for large ω approaches the constant value $\omega^{1/2}r=3.515\,846$ appropriate for the imageless pattern.

Clearly, for all practical purposes the images may be omitted for ω somewhat greater than ω^*. Fortunately, R/a for helium is usually so large that the value of ω at which a particular pattern will be the equilibrium state, or close to it, is always appreciably greater than ω^* for that pattern. The effect of the images is to decrease the free energy by about the same amount for patterns of the same N and ω so the error (caused by omitting the images) in the energy difference *between* patterns will be even less than indicated in the third column of Table I. For noncircular boundries the images are undoubtedly more important.

III. RESULTS FOR SINGLE PATTERNS

A. Energies and ring numbers

To systematically determine the stable vortex patterns we did the following: For the initial configurations we distributed the vortices in various rings, having found that random configurations did not efficiently produce patterns of higher free energy. We transformed these into stable patterns using the iterative procedure described earlier, with u_k from Eq. (4). For each value of N we tried many different initial configurations and believe that we found most, and possibly all, stable patterns. Because patterns of higher free energy are generally less stable and harder to find, any patterns we may have missed probably belong to this type and should not be as physically important as the patterns of lowest free energy. We calculated Δf_0 for each pattern and ordered the patterns in increasing Δf_0. We did this for $N=1,2,\ldots,30,37$, and 50. Also, for $N=61$, 91, 127, 169, and 217 we calculated the two lowest-energy patterns. All these results are listed in Table II. In a few cases, such as $N=50$, the patterns converged so slowly that the last digit in Δf_0 may only be an upper bound.

We generated computer-drawn pictures of all of the patterns. For example, the seven patterns that we found for $N=18$ are pictured in Fig. 1; the pictures for all values of N are published in a separate report.[9] Below each pattern in Fig. 1 is listed the corresponding value of Δf_0. These plots are for the low value $\omega=26$ so that the patterns are large, but they can be scaled to any size using the relation $\omega r_i^2=\text{const}$. The ring structure mentioned earlier is quite evident in these pictures. For example, pattern 18_1 has one vortex apparently in the center, surrounded by an apparent ring of six vortices, which is surrounded by another apparent ring of eleven vortices. Because of the asymmetry of this arrangement, neither of these rings can be exact in the sense that the radii of the vortices are identical, nor can the first vortex be precisely at the center. Still, these ring numbers give a useful means of describing and identifying the patterns. We determined these numbers for all the patterns using the criterion that two vortices fall in the same ring if their radii agree within 2% for $N<50$, and 5% for $N>50$, which gives sufficiently simple yet unique labels for most patterns. These ring numbers, ordered from the center of the patterns, are included in Table II and are listed below Δf_0 in Fig. 1. Patterns 18_3 and 18_5 have unusual centers with two "rings" of three vortices just slightly different in radius. In each of these rings the three vortices are symmetrically placed on a perfect circle. This center structure is then surrounded by an approximate ring of twelve vortices. The difference between these two patterns, which have identical ring numbers according to our 2% criterion, is a rotation of the outermost ring with respect to the center. In 18_3 the second (larger) ring of three vortices is aligned directly with three vortices of the outside ring of twelve, while in 18_5 the second ring is aligned with spaces in the outside ring. In patterns 18_4 and 18_6 we have a similar situation with the six in the center lying on a perfect circle. The type of "degeneracy" manifest in these two pairs of patterns occurs only in patterns whose ring numbers are commensurate and allow such high symmetry.

The patterns designated by the letter X in Table II are a sample of the many we found to be "nearly" stable. That is, an appropriate initial configuration would show good convergence in all quantities, yet upon further iteration this apparently stable pattern would eventually reveal its instability and move to another pattern which, itself, could be either stable or

TABLE II. Free energies Δf_0, with respect to the triangular continuum model, of stationary patterns of N quantized vortices in an unbounded, rotating fluid. The ring numbers are the numbers of vortices having approximately the same distance from the axis of rotation, in order of increasing distance. The patterns denoted by X represent a few of the stationary patterns that are known to be nearly stable, as opposed to stable. For $N \leq 30$, $N = 37$ and 50, the listing of stable and stationary patterns is complete, to our knowledge. The units of Δf_0 are $\rho\kappa^2/4\pi$.

N	Order	Δf_0	Ring Numbers
1	1	−0.001 25	1
2	1	0.190 65	2
3	1	0.144 18	3
4	1	0.107 40	4
5	1	0.133 07	5
	2	0.403 65	1, 4
6	1	0.217 81	1, 5
	2	0.249 27	6
7	1	0.107 49	1, 6
	2X	0.473 84	7
8	1	0.094 54	1, 7
9	1	0.194 05	1, 8
	2	0.266 94	2, 4, 3
	3X	0.267 16	2, 3, 4
	4X	0.543 66	3, 6
10	1	0.224 33	2, 4, 4
	2X	0.225 78	2, 2, 4, 2
	3X	0.417 05	1, 9
11	1	0.249 18	3, 8
	2	0.288 59	2, 9
12	1	0.193 44	3, 3, 6
	2X	0.198 37	3, 6, 3
	3	0.350 22	4, 8
13	1	0.224 32	4, 9
	2	0.246 36	3, 10
14	1	0.177 90	4, 10
	2	0.367 13	5, 9
15	1	0.234 13	4, 11
	2	0.247 11	5, 10
	3X	0.247 73	5, 10
16	1	0.219 59	5, 11
	2	0.364 91	1, 5, 10
	3X	0.386 47	1, 5, 5, 5
	4	0.398 42	4, 4, 8
	5X	0.405 41	4, 8, 4
17	1	0.283 94	1, 5, 11
	2	0.294 12	5, 12
	3	0.348 94	3, 3, 11
	4	0.396 82	1, 6, 10
	5	0.474 07	1, 4, 4, 8
18	1	0.252 41	1, 6, 11
	2	0.283 16	1, 5, 12
	3	0.351 10	3, 3, 12
	4X	0.352 15	6, 12
	5X	0.352 41	3, 3, 12
	6X	0.356 26	6, 12
	7	0.477 28	5, 13
19	1	0.186 26	1, 6, 6, 6
	2X	0.193 17	1, 6, 12
	3	0.333 23	1, 7, 11
	4	0.380 32	1, 5, 13
	5	0.454 81	3, 3, 13
20	1	0.219 55	1, 6, 13
	2	0.219 60	1, 7, 12
	3X	0.436 85	2, 2, 4, 12
	4X	0.468 97	2, 4, 2, 6, 4, 2
21	1	0.190 96	1, 7, 13
	2	0.347 93	1, 6, 6, 8
	3	0.376 28	1, 4, 4, 12
	4	0.395 90	2, 2, 2, 3, 12
22	1	0.251 22	1, 7, 7, 7
	2X	0.263 11	1, 7, 14
	3	0.304 26	1, 8, 13
	4	0.333 39	2, 7, 13
23	1	0.313 90	1, 8, 14
	2	0.337 04	2, 2, 4, 2, 13
	3	0.338 01	2, 2, 2, 3, 14
	4	0.421 58	1, 7, 15
24	1	0.300 37	2, 2, 4, 2, 14
	2	0.397 88	3, 8, 13
	3	0.419 61	1, 8, 15
	4	0.446 24	1, 1, 2, 2, 3, 15
	5	0.448 89	2, 2, 2, 4, 1, 13
25	1	0.329 80	3, 8, 14
	2	0.352 68	2, 2, 4, 2, 15
	3	0.353 01	2, 2, 4, 2, 15
	4	0.377 05	2, 2, 7, 14
	5	0.425 24	2, 1, 3, 6, 13
	6	0.611 99	1, 8, 8, 8
26	1	0.317 62	3, 3, 6, 14
	2	0.332 69	3, 8, 15
	3	0.381 72	2, 1, 2, 6, 15
	4	0.486 66	2, 2, 4, 2, 8, 8

TABLE II. (Cont'd.)

N	Order	Δf_0	Ring Numbers
27	1	0.276 72	3, 3, 6, 15
	2	0.387 16	4, 9, 14
	3	0.409 83	3, 8, 16
	4	0.412 01	3, 4, 6, 14
	5*X*	0.438 07	3, 8, 16
	6	0.474 19	2, 1, 2, 6, 16
28	1	0.320 73	4, 9, 15
	2	0.324 82	3, 3, 6, 16
	3	0.342 32	3, 5, 5, 15
	4	0.343 11	3, 10, 15
	5	0.406 99	4, 4, 6, 14
	6	0.439 42	4, 8, 8, 8
	7*X*	1.344 75	1, 9, 18
29	1	0.311 63	4, 10, 15
	2	0.323 40	4, 9, 16
	3	0.345 97	3, 3, 7, 16
	4	0.459 88	3, 3, 6, 17
30	1	0.276 72	4, 4, 6, 16
	2	0.394 29	4, 11, 15
	3	0.405 88	5, 5, 5, 15
	4	0.407 38	4, 9, 17
	5	0.435 43	3, 3, 7, 17
37	1	0.284 24	1, 6, 6, 6, 18
	2	0.288 84	1, 6, 6, 6, 18
	3	0.398 54	1, 7, 12, 17
	4	0.419 83	1, 6, 11, 19
50	1	0.441 56	4, 10, 15, 21
	2	0.452 44	4, 9, 16, 21
	3	0.464 82	3, 3, 6, 16, 22
	4	0.480 20	3, 3, 7, 15, 22
	5	0.491 86	4, 4, 6, 16, 20
	6	0.543 19	3, 3, 6, 9, 6, 23
	7	0.620 67	3, 2, 2, 6, 17, 20
61	1	0.397 58	1, *j*6, $1 \leq j \leq 4$
	2	0.421 73	1, *j*6, $1 \leq j \leq 4$
91	1	0.536 80	1, *j*6, $1 \leq j \leq 5$
	2	0.586 31	1, *j*6, $1 \leq j \leq 5$
127	1	0.703 45	1, *j*6, $1 \leq j \leq 6$
	2	0.782 94	1, *j*6, $1 \leq j \leq 6$
169	1	0.898 30	1, *j*6, $1 \leq j \leq 7$
	2	1.011 67	1, *j*6, $1 \leq j \leq 7$
217	1	1.122 14	1, *j*6, $1 \leq j \leq 8$
	2	1.272 48	1, *j*6, $1 \leq j \leq 8$

nearly stable. It seems clear that the nearly stable patterns correspond to saddle points in the free energy and it is only by the accumulation of computer round-off error that sufficient amplitude is given to their unstable degree of freedom to permit further decrease in free energy. There are probably additional nearly stable patterns among the "stable" ones listed in Table II, especially at higher N.

These stable arrays are the result of the two competing effects. First, the vortices effectively repel each other and try to stay apart and, second, the pattern would like to be round and compact. This can be seen by thinking of the u_k in Eq. (4) as the force on each vortex, as these are zero for the stable patterns. The first term represents a pair-wise repulsive interaction which drops off as $1/r$ while the second is a harmonic-like attraction to the axis of the bucket with strength proportional to ω. Note that the image term, the second in Eq. (3), has the opposite sign and therefore the vortices attract their images.

As N increases, the pattern with lowest free energy changes from 1 in the center to 2,3,4,5, and then back to 1 ($N=16$), 2 ($N=10$), 3, 4, 5, and again 1 ($N=17$). This cycle then repeats. Having 1 vortex in the center of the lowest energy pattern is presumably a property of vortex numbers close to those with "triangular" ring numbers,
$N=1+6(1+2+3\cdots)=1, 7, 19, 37$, etc.

B. Equilibrium thresholds

The free energy of each pattern as a function of ω is given by $f_0(N,\omega)=f_c(N,\omega)+\Delta f_0$. To find the equilibrium patterns for a range of values of ω, we could plot all these curves as a function of ω (for a given value of R/a). Each curve would be fairly straight, become negative very quickly, and intersect all other curves. The locus of all equilibrium states would be the union of all the segments that form the bottom envelope of all these free-energy curves. Such a plot, however, would not be very convenient because f_0 varies tremendously and the curves would be too close to distinguish intersections. To make a more useful plot we subtract from each curve f_0 a function of ω that approximates the lower envelope of those curves, which does not affect the relative values of free energy at each value of ω, and then magnify the vertical scale to show the fine structure in free energy. For this function we use $f_c(N_0,\omega)$ where $N_0(\omega)$ is the value of N which minimizes $f_c(N,\omega)$ for each ω. It is determined by the condi-

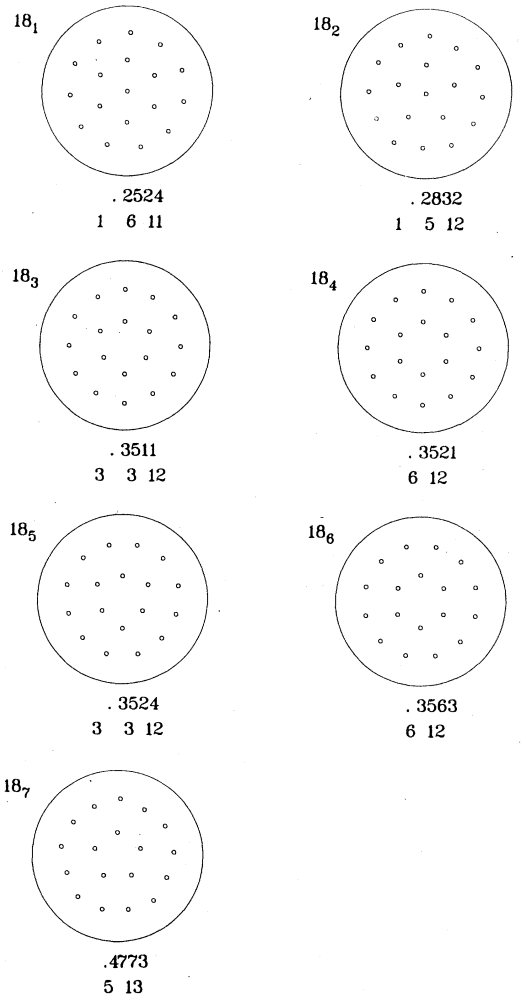

FIG. 1. Seven stationary patterns of 18 vortices for $\omega = 26$. Immediately below each pattern is the corresponding value of Δf_0 and the ring numbers, both of which are independent of ω.

tion

$$\left[\frac{\partial f_c(N,\omega)}{\partial N}\right]_{N=N_0} = 0 \ , \tag{10}$$

where

$$\frac{\partial f_c(N,\omega)}{\partial N} = N - N\ln N - \omega + (N-\tfrac{1}{2})\ln\omega - b + \ln\left(\frac{R}{a}\right) \ . \tag{11}$$

Although this is a transcendental equation, it is not difficult to solve numerically by iteration.[10] Then for each pattern we plot the function

$$g(N,\omega) \equiv f_0(N,\omega) - f_c(N_0(\omega),\omega) = f_c(N,\omega) - f_c(N_0(\omega),\omega) + \Delta f_0 \ . \tag{12}$$

As a function of ω, each of these curves has a minimum at $\omega_0(N)$ determined by

$$\left[\frac{\partial g(N,\omega)}{\partial \omega}\right]_{\omega=\omega_0} = 0 \ , \tag{13}$$

which is zero when

$$\partial f_c(N,\omega_0)/\partial N = 0 \ . \tag{14}$$

For each N, $\omega_0(N)$ depends only upon the parameter R/a. These curves are plotted in Figs. 2(a)–2(c), for $0 \leq N \leq 30$ and $0 \leq \omega \leq 70$, for the particular value $R/a = 10^7$ and in Fig. 3 for $48 \leq \omega \leq 53$. The exact results of Fig. 2 can be closely approximated by expanding Eq. (12) to second order about ω_0; making use of Eq. (11) we find the parabolas

$$g(N,\omega) \approx \Delta f_0 + \frac{1}{2}\left(\frac{\omega-\omega_0}{\omega_0}\right)^2 \frac{(\omega_0 - N + \frac{1}{2})^2}{\ln(\omega_0/N)} \ . \tag{15}$$

From Fig. 2 the equilibrium states can be determined. For example, centered directly above $\omega = \omega_0(18) = 49.7$, a value determined by Eq. (13), are nested the seven parabola-like curves for $N = 18$, not all of which can be distinguished. This is shown on a more expanded scale in Fig. 3. The minimum of each of these is at Δf_0, as given in Table II. Except for this additive constant, the seven curves are identical, according to Eqs. (12) or (15). The lowest of these, for pattern 18_1, has the smallest free energy of any pattern for $48.8 \leq \omega \leq 50.4$, and so in this range it is the stable, equilibrium one. At $\omega = 50.4$ this curve intersects the curve for pattern 19_1, so, for larger ω, 19_1 is the stable pattern. Clearly, patterns 18_2 and $18_3, \ldots, 18_7$ can never be equilibrium states. They may exist as metastable states and those that are absolutely stable may have indefinitely long lifetimes. At any $\omega < 70$, the free-energy difference between the various patterns can be read off Figs. 2 or 3.

The change from N to $N+1$ vortices in the equilibrium pattern occurs at the value of ω where adjacent parabolas intersect, i.e., where $g(N,\omega) = g(N+1,\omega)$. In Fig. 4 we give these transition values of ω for $0 \leq N \leq 30$, $0 \leq \omega \leq 60$, and $10^2 \leq R/a \leq 10^{10}$. This is an extension of a similar plot by Hess,[3] who went as far as $N = 8$. Although for practical values of R/a this figure summarizes the equilibrium behavior, the physical transitions between patterns as ω is changed will not necessarily occur at exactly the values in Fig. 4 because of the energy barrier between patterns of different N. Note that the lines on this plot are not evenly spaced, a result of the varying values of f_0 as evident in Fig. 3. However, because the bottom of the parabolas in Figs. 2 and 3 are at $\omega_0(N)$, determined by the continuum model, the general behavior of Fig. 4 is well approximated by that model, as shown by the dashed lines for $N > 30$. For a given ω, the value $N_0(\omega)$ determined by the continuum model, namely, Eqs. (10) and (11), can differ from the equilibrium N by at most ± 1.

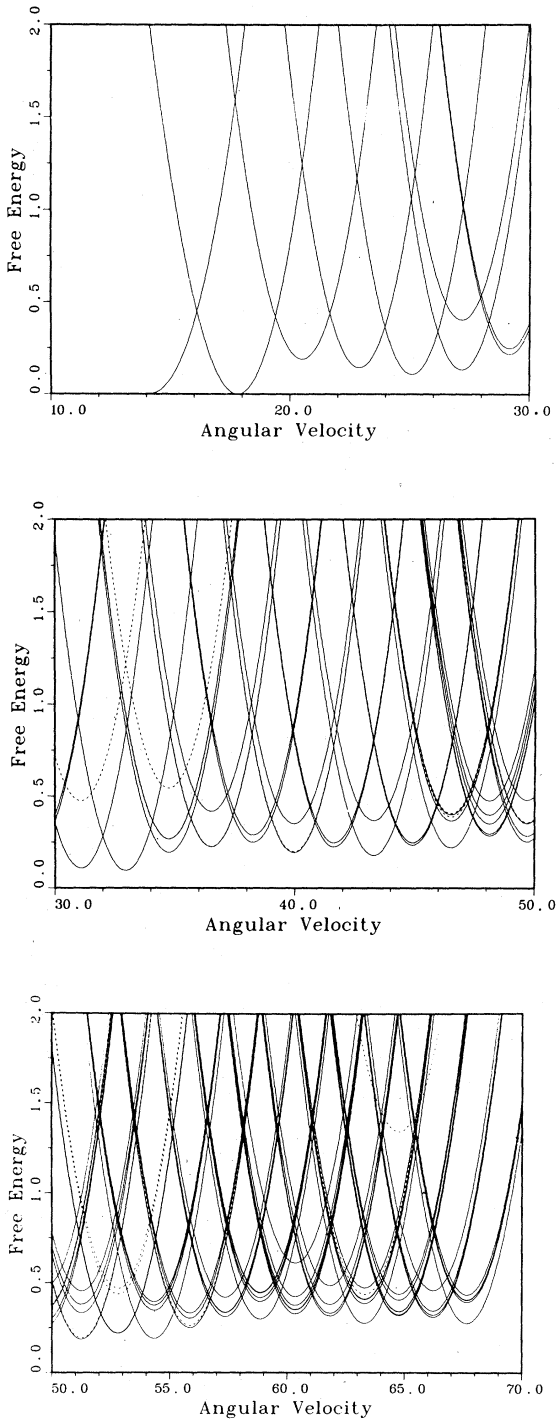

FIG. 2. Free energy of rotating superfluid with 0 to 30 vortices relative to the continuum free energy $f_c(N_0(\omega), \omega)$ for $R/a = 10^7$. The first curve on the left is for no vortex, to its right is that for a single vortex, etc. Dashed lines denote nearly stable patterns.

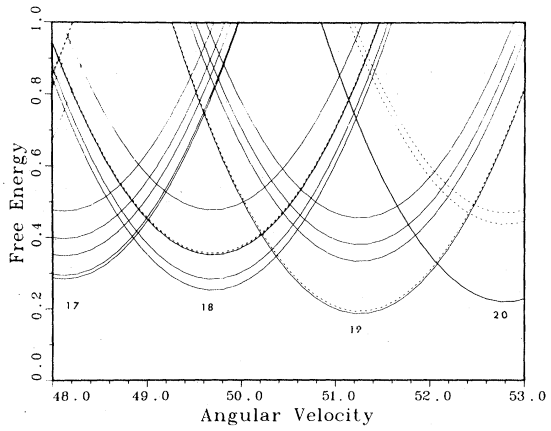

FIG. 3. Interval $48 \leq \omega \leq 53$ of Fig. 2 showing the free energy for patterns of 17 through 20 vortices.

C. Circular distortion

Patterns containing triangular numbers of vortices, $1+3j(j+1)$, were studied because they favor a triangular lattice, the lowest energy configuration of an infinite number of vortices. Strictly speaking, the numbers of vortices that most favor triangular arrays

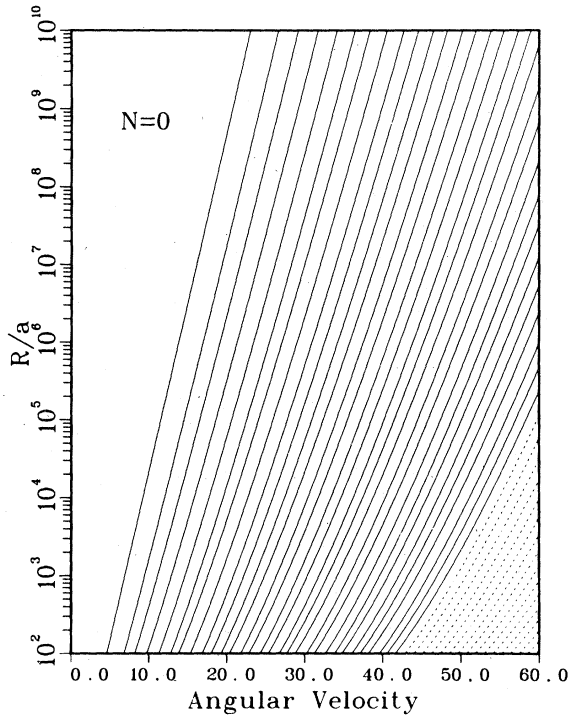

FIG. 4. Values of angular velocity ω, as a function of R/a, at which the number of vortices in the equilibrium pattern changes. For example, the left-most line gives the value of ω at which a single vortex and no vortex have the same free energy. The dashed lines were calculated from the continuum model for $N > 30$.

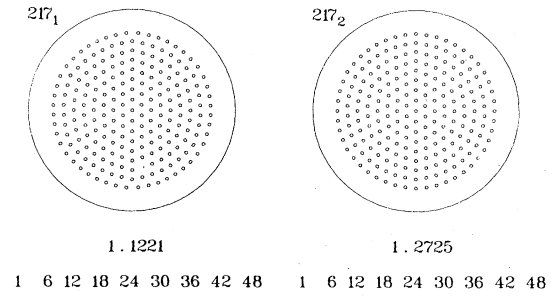

FIG. 5. Lowest energy patterns for $N=217$.

are ambiguous for arrays with radii larger than six vortex spacings ($j>6$) because such circles contain more lattice points than do hexagons of the same radius. (The number chosen is not particularly important because it is shown in Appendix C that finite triangular lattices lack stability.) We find the lowest energy pattern has the outer ring rotated by half a vortex spacing compared to a more triangular pattern of slightly higher energy. Moreover, we find that circular distortion penetrates deeply into the patterns and destroys triangular symmetry in at least half the area of the pattern. From the evidence of patterns up to $N=217$, which is shown in Fig. 5, this distortion appears to occur in a fixed fraction of the area rather than in a surface layer. This is probably related to the fact that the free-energy difference per vortex $\Delta f_0/N$ seems to be approaching a nonzero limit, as shown in Table III. For comparison, the energy difference per vortex between the infinite square and triangular lattices is 0.010 58. We emphasize that the above circular distortion effects are in no way attributive to the influence of a boundary; our omission of images gives results for an unbounded fluid.

To show that this circular distortion is not, overall, a small perturbation upon triangular symmetry, we display the scattering structure factors $S(Q)$ for patterns 217_1 and 217_2 in Fig. 6. For comparison, $S(Q)$ for a circular region of a perfect triangular lattice of 211 vortices is shown in Fig. 7. The structure factor

TABLE III. Excess free energy per vortex in equilibrium patterns compared to an infinite triangular lattice.

N	$\Delta f_0(N)/N$
61	0.006 52
91	0.005 90
127	0.005 54
169	0.005 32
217	0.005 17

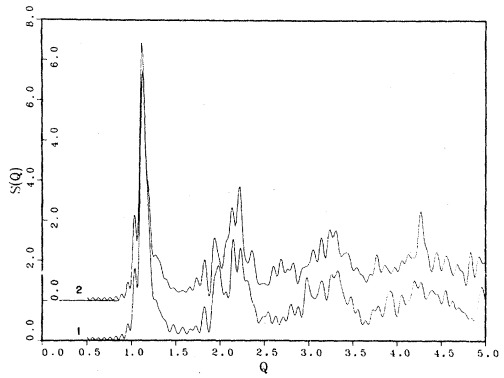

FIG. 6. Scattering structure factor for patterns 217_1 (lower) and 217_2 (upper). Q is in units of $2\pi/\lambda$ where λ is nearest-neighbor distance.

we used is

$$S(Q)=\frac{1}{2\pi N}\int_0^{2\pi}d\theta\left|\sum_{j=1}^{N}e^{iQr_j\cos(\theta-\theta_j)}\right|^2, \qquad (16)$$

proportional to the average scattering intensity for a rotating sample and a fixed incident beam. The wave number Q is in units of $2\pi/\lambda$ where λ is the minimum nearest-neighbor distance among the five vortices closes to the center of the pattern. These figures show not only the limited extent of triangular symmetry in finite, stable vortex arrays but also the resolution that will be required to distinguish arrays of the same N by scattering experiments.

It might be thought that the ciruclar distortion is a property only of small vortex arrays and that larger triangular arrays would be stable. We consider this possibility in Appendix C where we find that a vortex at position R in such an array of radius R_0 is subject to a destabilizing velocity that varies as $(R/R_0)^5$. Because we see no significant deviation from this result for arrays containing up to one million vortices we doubt that any finite circular region of a triangular

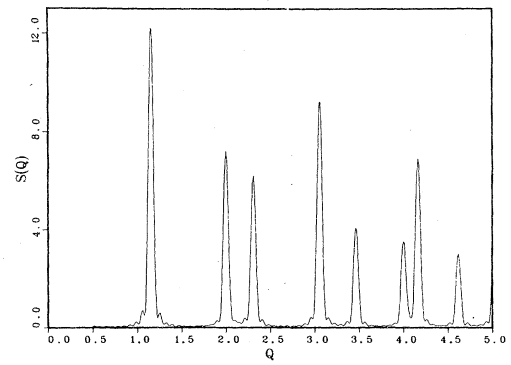

FIG. 7. Scattering structure factor for a circular section of a perfect triangular lattice containing 211 vortices.

lattice (containing more than seven vortices) is stable; i.e., distortion seems necessary for stability.

IV. FREE-ENERGY BARRIERS BETWEEN STABLE PATTERNS

A. Barriers between patterns of the same number of vortices

By definition, any small deviation of the vortices from their positions in a stable pattern of N increases the free energy. Therefore a trajectory consisting of N vortex positions $z_i(s)$ as a function of some parameter will define a free energy $f(z_i(s))$ which has a maximum when the trajectory connects two stable patterns. This maximum is a saddle point in the free energy of N unconstrained vortices. The problem is to find a trajectory, of all possible trajectories connecting two stable patterns, that has the smallest maximum. Such a trajectory will be called optimum, whether or not it is unique. We consider as self-evident the existence of at least one optimum trajectory for any two stable patterns. (However, if images are included and $\omega \approx \omega^*$ then a pattern may not tolerate distortion without losing vortices to the boundary.)

The method we use to find optimum trajectories consists of constraining a particular vortex to move from its position in one stable pattern to a position consistent with the known vortex positions of the second stable pattern. The arc length of the path of the constrained vortex becomes the parameter s. After each increment $s + ds$ of the constrained vortex, the remaining $N = 1$ vortices are allowed to converge to a local minimum in the free energy. Because of cylindrical symmetry we need to consider only radial motion of the constrained vortex; any angular motion of the constrained vortex would merely cause overall rotation of the pattern.

Not every choice of constrained vortex or its final position results in an optimum trajectory. If the final vortex position, equal to a known vortex radius of the second pattern, differs but little from the initial position then the second pattern will not, in most cases, be achieved by that trajectory. Instead, the result will merely be a distortion of the first pattern that corresponds to no stable pattern of N vortices.

Some choices of constrained vortex result in a discontinuous trajectory in the sense that the free energy, as a function of the position of the constrained vortex, develops a saddle point in the space of the $N-1$ vortices. When this instability is reached the $N-1$ vortices abruptly switch to a new configuration. Reversing the direction of the constrained vortex after passing through such an instability will not necessarily return the system to the initial pattern. If it does, then the singularity is again passed but at a different value of the position s. These features are illustrated in Figs. 8 and 9 which show calculations, without images, of the free energy (solid line) and angular momentum (dashed line) as functions of the

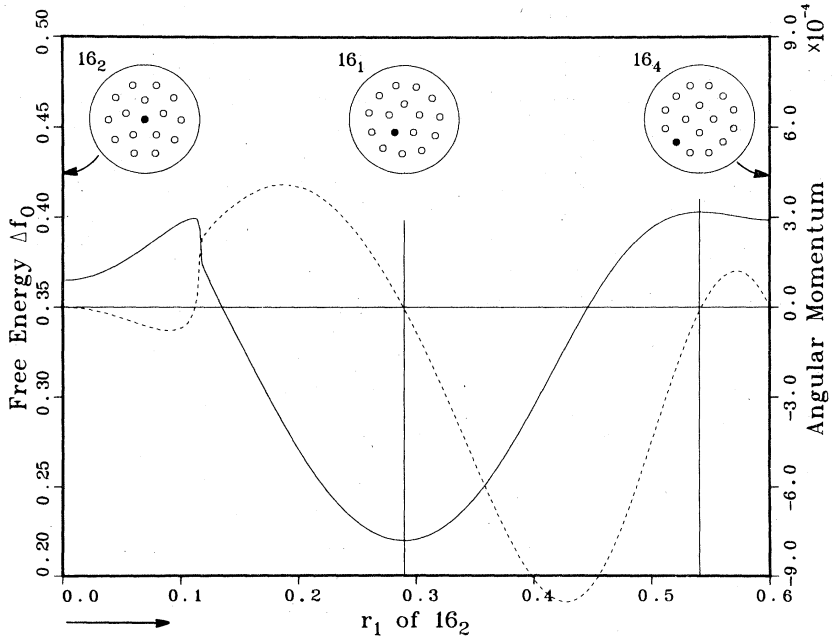

FIG. 8. Variation of free energy (solid line) and angular momentum (dashed line) as the center vortex r_1 of 16_2 is moved outward. The array changes from 16_2 to 16_1 and then to 16_4 with intervening stationary saddle points, the first of which is discontinuous. The angular momentum is given as the fractional deviation from the equilibrium value in units of 10^{-4}.

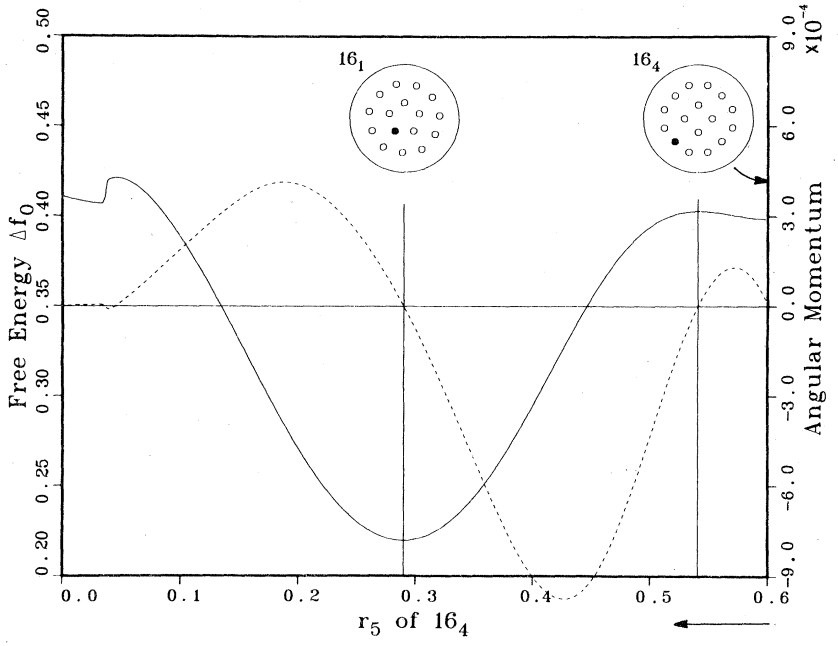

FIG. 9. This is similar to Fig. 8 except r_5 of 16_4 is moved inward. Here the array at $r_5 = 0$ corresponds to no stable pattern.

radial position of the constrained vortex. In Fig. 8 the constrained vortex is number 1 (vortices are ordered by their distance from the origin in the initial pattern) and the initial pattern is 16_2. As its radius r_1 increases from zero an instability is encountered at $r_1 = 0.11$ after which pattern 16_1 is obtained at $r_1 = 0.29$ and then pattern 16_4 at $r_1 = 0.60$. Reversing this process, i.e., starting with vortex number 5 of pattern 16_4, the same curve is obtained in Fig. 9 until the vicinity of the singularity, which here occurs at $r_5 \approx 0.04$. Note that pattern 16_2 is not recovered after passing through the singularity; the configuration at $r_5 = 0$ corresponds to no stationary pattern of 16 unconstrained vortices.

Does there always exist an optimum trajectory that is continuous? We cannot answer this question definitively but, in practice, we have never failed to find one. For example, a continuous trajectory, which we believe is optimum, occurs between 16_2 and 16_1 when vortex number 6 of 16_2 is chosen as the constrained vortex. Within the accuracy of the calculation the barrier energies of this continuous trajectory and the discontinuous trajectory of Fig. 8 are equal.

For some pairs of patterns there is no optimum trajectory that does not pass through a third stable pattern. For example, 15_2 and 15_3 can be connected by an optimum trajectory only through 15_1. Also, for some patterns it is possible to choose a constrained vortex that results in a trajectory connecting the pattern to itself, without passing through another stable pattern.

The angular momenta of the trajectories are shown in Figs. 8 and 9 to illustrate that all stable and saddle-point patterns have the same angular momentum. (The converse is not true; a vortex configuration with the same angular momentum as a stable pattern is not necessarily either stable or a saddle point.) The vertical lines in the figures emphasize the correspondence between free energy and fixed angular momentum. Note that the deviation of the angular momentum over the trajectories is less than 0.1%.

A list of some barrier energies for $N \leq 20$ is given in Ref. 11.

B. Barriers between patterns of different numbers of vortices

We consider the barrier energy (defined, of course, only in the presence of images) for the entrance of an additional vortex to a system of N vortices. This applies to systems in angular acceleration. (For angular deceleration, the pattern grows in size until ω^* is reached; one or more vortices then leave at the boundary.) To derive an accurate estimate of this barrier energy we use Eq. (1) to write the general free energy of $N+1$ vortices in terms of that of N vortices,

$$f(N+1)=f(N)-\sum_{i=1}^{N}\ln(r_i^2+r_{N+1}t^2-2r_ir_{N+1}\cos\theta_i)+\sum_{i=1}^{N}\ln(1+r_i^2r_{N+1}^2-2r_ir_{N+1}\cos\theta_i)$$

$$+\ln(1-r_{N+1}^2)-\omega(1-r_{n+1}^2)+\ln(R/a) \quad . \tag{17}$$

In the spirit of the continuum model we approximate the N vortices by a uniform density of vortices in a circle of radius r. Note that we assume the pattern of the N vortices is not distorted by the added vortex. The two sums in Eq. (17) then become integrals; the first gives $N\ln r_{N+1}^2$ and the second vanishes (because a single vortex has zero interaction with the images of a circular, continuous distribution of vorticity). Equation (17) becomes

$$f(N+1)\approx f(N)+\ln(1-r_{N+1}^2)-N\ln r_{N+1}^2$$
$$-\omega(1-r_{N+1}^2)+\ln(R/a) \quad . \tag{18}$$

The barrier free energy $f_b(N+1)$ is the maximum of $f(N+1)$ as a function of r_{N+1}. This occurs for $r_{N+1}=r_b$ where

$$r_b^2=\frac{1}{2}\left[1+\frac{N-1}{\omega}\right.$$
$$\left.+\left\{\left[1-\frac{1}{\omega}\right]^2+\frac{N}{\omega}\left[\frac{N}{\omega}-2\left[1+\frac{1}{\omega}\right]\right]\right\}^{1/2}\right] \quad . \tag{19}$$

Note that $r_b<1$ for $\omega<\infty$. Whether or not one uses the continuum-model approximation for $f(N)$ in Eq. (18) makes little difference because that error is roughly comparable to ignoring pattern distortion. Comparison of both the barrier energy and r_b from Eqs. (18) and (19) with full pattern calculations of these quantities showed good agreement; for example, less than 0.5% error for $N=21$ and $\omega=30$. This supports the assumption that the pattern of N vortices is relatively undistorted by the presence of an additional vortex near r_b, provided that ω is not near ω^*.

This barrier energy is relatively high and, by itself, would strongly inhibit the entrance of vortices into rotating helium. The classical condition for transition between states of N and $N+1$ vortices is $f_b(N+1)=f(N)$ which may occur for $\omega>>1$ and $N/\omega<1-1/\omega^{1/2}$. Equations (18) and (19) then give $(y=N/\omega)$

$$r_b^2\approx 1-\frac{a}{R}e \quad , \tag{20}$$

$$\omega\approx\frac{R}{a}/[e(1-y)] \quad . \tag{21}$$

That is, the transition cannot occur unless the angular velocity is of order R/a and the $N+1$ vortex is nucleated within a core radius of the boundary. This is essentially the same result known for many years from the early hydrodynamic predictions of critical velocities and, like the latter, is in substantial disagreement with experiment.[12] In particular, if the above hydrodynamic barrier energy dominated the nucleation of vortices then there would be a large hysteresis in the observed number of vortices as ω is increased and decreased. Although hysteresis is seen in the experiments, indicating the presence of some barrier energy, it is less than what the above hydrodynamic barrier energy would predict. One physical feature outside this two-dimensional theory of the barrier energy is the three-dimensional possibility for vortices to grow continuously to their full length rather than to abruptly nucleate along the full length of the container. Perhaps experimental conditions will be found which will permit detection of the hydrodynamic barrier energy derived here.

V. SUMMARY

Except for features of transitions between states of different vortex number, such as the barrier energy for vortex entrance at the boundary or the critical angular velocity for pattern stability, the properties of vortices in a cylindrical container are not appreciably influenced by the images. Omitting the images leads to useful simplification in the formula for the free energy f. In particular, the ω (angular velocity) dependences of the "imageless" free energy f_0 and the continuum-model free energy f_c become simple and identical; therefore free energies can be expressed relative to the continuum model as $\Delta f_0=f_0-f_c$, thereby removing all dependence on ω. (An equivalent definition is $\Delta f_0=\lim_{\omega\to\infty}f-f_c$.) This permits the assignment of a unique energy number to each stable vortex pattern. The omission of images also permits an exact evaluation of the angular momentum of any stable or saddle-point pattern, which is a useful absolute criterion for the numerical convergence of patterns and which leads to an accurate estimate of pattern sizes, including the radii of the interior rings. The dimensions of stable, imageless patterns scale exactly with ω as $\omega^{1/2}r$.

The energies, ring numbers, and pictures[9] of 125 patterns for $N\leq 30$ and $N=37$, 50, 61, 91, 127, 169, and 217 provide a data base for studying the relative energies of patterns and their systematics. Because of hysteresis due to barrier energies the experimentally observed number of vortices is dependent on the history of angular acceleration or deceleration. However, the equilibrium number is well defined and is graphed in Fig. 4. For a typical value of R/a, Figs.

2 and 3 show the fine structure of pattern energies as a function of ω.

The pictures of patterns which favor triangular symmetry, $N=61$, 91, etc., suggest that circular distortion of the triangular symmetry persists in about half the total area of any finite pattern. Likewise, the trend in $f_0(N)$ as N increases suggests there is an additional energy factor proportional to N for any finite number of vortices compared to the same number of vortices in an infinite triangular lattice.

The lowest free-energy saddle point for transitions between patterns of the same n can be calculated by constraining an appropriate vortex to move radially. In the absence of images the angular momentum is identical for all stable and saddle-point patterns and changes less than 1% during transitions between patterns. The free-energy barrier for the entrance of an additional vortex in an two-dimensional system can be accurately estimated and is much higher than is observed in experiments on manifestly three-dimensional helium.

The system of quantized vortices considered here belongs to the small class of idealized systems such as the Bose gas, Fermi gas, harmonic oscillator, etc., which have, throughout the history of physics, fruitfully illuminated the understanding of physical systems, served to illustrate general principles, and provided a testing ground for new theories and methods. For the vortex system we are fortunate in having as close a physical representation as rotating superfluid ^{4}He. Other systems that are described, in important respects, by equations identical to those used here are parallel line changes in a circular cylinder of uniform charge (of the opposite sign) and screw dislocations in a circular crystal under torsion.

Note added in proof. The observation of many of the features of vortex patterns discussed here has just been reported by Yarmchuk, Gordon, and Packard.[18] Included in their Letter are photographs of patterns for $N=1$ to 11, which clearly show the tendency for rings to form, and which are consistent with our predicted configurations.[9] For $N=6$, they observed the metastable 6_2 pattern as well as the stable 6_1 one, while for all other N, up to 11, only the stable patterns were seen. The absence of the metastable patterns for $N=5$ and 9 reflects the high energy these patterns have with respect to their stable counterparts (see Table II).

ACKNOWLEDGMENT

This work was supported by the U. S. DOE Contract No. W-7405-ENG-36.

APPENDIX A

We present here a proof of the angular-momentum relation, Eq. (5). The first term is obvious. For the second we have

$$\sum_{k=1}^{N}\omega r_k^2=\sum_{k=1}^{N}\omega z_k\bar{z}_k=\sum_{k=1}^{N}\sum_{j=1}^{N}{}'\frac{\bar{z}_k}{\bar{z}_k-\bar{z}_j}\ , \tag{A1}$$

where we use Eq. (4) with $u_k=0$, so that the result will only be valid for configurations which make f stationary. Because we sum on both j and k we may write the last term above

$$\frac{1}{2}\sum_{k=1}^{N}\sum_{j=1}^{N}{}'\left(\frac{\bar{z}_k}{\bar{z}_k-\bar{z}_j}+\frac{\bar{z}_j}{\bar{z}_j-\bar{z}_k}\right)=\frac{1}{2}N(N-1)\ , \tag{A2}$$

since the summand is unity. This proves Eq. (5).

APPENDIX B

Here we fully derive the free energy of the continuum model. Because the distribution of vortices is nearly uniform, we can approximate the double sum in Eq. (7)

$$-\frac{1}{2}\sum_{i\neq j}^{N}\ln\omega|z_i-z_j|^2\ , \tag{B1}$$

by the integral,

$$-\frac{1}{2}\left(\frac{N}{\pi r_c^2}\right)^2\sum_{i=1}^{N}\int_{|\vec{r}|<r_c}d\vec{r}\ln(\omega|\vec{r}_i-\vec{r}|^2)$$
$$=-N^2(\ln\omega^{1/2}r_c-\tfrac{1}{4})-\tfrac{1}{2}N\ . \tag{B2}$$

We assume that all vortices lie within a circle of radius r_c, which is determined by the requirement that the average vorticity $N\kappa/\pi(r_cR)^2$ (in physical units) is equal to 2Ω. In terms of the dimensionless angular velocity ω, this gives

$$r_c=(N/\omega)^{1/2}\ . \tag{B3}$$

The difference between Eqs. (B1) and (B2) is the difference between the sum and integral of $-\ln\omega|\vec{r}_i-\vec{r}_j|^2$. The major contribution to that difference comes when $\vec{r}_i$ and $\vec{r}_j$ are close; therefore we can approximately take the lattice to be infinite and let one summation and one integration be unbounded. Then the other summation and the other integration can both be performed to give exactly N and we are left with

$$-\frac{N}{2}\lim_{\alpha\to 0}\left(\sum_{\vec{r}}{}'\ln\omega r^2e^{-\alpha\omega^{1/2}r}-\frac{\omega}{\pi}\int d\vec{r}\ln\omega r^2e^{-\alpha\omega^{1/2}r}\right)$$
$$\equiv -Nb\ . \tag{B4}$$

The exponential factor is inserted to allow the sum and integral to converge separately. We also made use of Eq. (B3). Thus, we approximate the sum (B1) by the two terms (B2) and (B4). This gives exactly the expression Eq. (8) for f_c. The next correction would be a surface term of order $N^{1/2}$. Now we must evaluate b.

The sum in Eq. (B4) is over all lattice points on an infinite lattice except for $\vec{r}=0$ (indicated by a prime on the summation). For a square lattice, we have

$$\omega r^2=\pi(n_1^2+n_2^2),\quad n_i=0,\pm1,\pm2,\ldots, \tag{B5}$$

and for a triangular lattice,

$$\omega r^2=\frac{2\pi}{3^{1/2}}(n_1^2+n_2^2+n_1n_2)\ ,\quad n_i=0,\pm1,\pm2,\ldots, \tag{B6}$$

The above coefficients are chosen so that the area per vortex is $\pi r_c^2/N=\pi/\omega$. For the square lattice the sum in Eq. (B4) is similar to certain sums that apply to the ideal Bose-Einstein gas, and the methods used in that problem[13] can be applied here for both lattices. We will study the function

$$f(\alpha,z)=\sum_{n_1,n_2}{}'\frac{e^{-\alpha P}}{P^{2z}}\ , \tag{B7}$$

where $P^2\equiv\omega r^2$ as given by either Eq. (B5) or Eq. (B6). The behavior about $\alpha=0$ can be found by use of the Mellin transform,

$$\begin{aligned}F(s,z)&=\int_0^\infty d\alpha\, f(\alpha,z)\alpha^{s-1}\\&=\sum{}'P^{-2z}\int_0^\infty d\alpha\, e^{-\alpha P}\alpha^{s-1}\\&=\Gamma(s)\Upsilon(z+s/2)\ ,\end{aligned} \tag{B8}$$

where

$$\Upsilon(k)\equiv\sum{}'P^{-2k},\quad k>1\ . \tag{B9}$$

This is a two-dimensional generalization of the ζ function. Analogous to Riemann's integral representation of that function,[14] one can derive the following representation of $\Upsilon(k)$:

$$\Gamma(z)\Upsilon(z)=\frac{1}{z-1}-\frac{1}{z}+\sum_{n_1,n_2}{}'[E_{1-z}(P^2)+E_z(P^2)]\ , \tag{B10}$$

where

$$E_n(x)=\int_1^\infty dt\, t^{-n}e^{-xt}=x^{n-1}\Gamma(1-n,x) \tag{B11}$$

is the form of the incomplete Γ function. This follows because for both lattices,[13,14]

$$\sum_{n_1,n_2}e^{-aP^2}=\frac{1}{a}\sum_{n_1,n_2}e^{-P^2/a}\ , \tag{B12}$$

which itself follows from the Poisson summation formula. The sum on the right of Eq. (B10) is convergent for all complex z, so this gives the analytic continuation of Eq. (B9) over the complex z plane. For example, we have the reflection formula $\Gamma(z)\Upsilon(z)=\Gamma(1-z)\Upsilon(1-z)$. Furthermore, because $\Gamma(z)$ has a simple pole at $z=0$, and no zeros, Eq. (B10) implies that $\Upsilon(z)$ has a simple pole at $z=1$ with residue 1. Using this we can invert the Mellin transform (B8). We have formally

$$f(\alpha,z)=\frac{1}{2\pi i}\int_{c-i\infty}^{c+i\infty}\Gamma(s)\Upsilon(z+s/2)\alpha^{-s}\,ds\ , \tag{B13}$$

where the contour is to the right of all singularities. The function $\Gamma(s)$ has simple poles at $s=-k$, $k=0,1,2\ldots$, with residue $(-1)^k/k!$, and $\Upsilon(z+s/2)$ has a simple pole at $s=2-2z$ with residue 2. We can deform the contour to encircle just the singularities. Starting from the right, we get the following development for $f(\alpha,z)$:

$$f(\alpha,z)=\frac{2\Gamma(2-2z)}{\alpha^{2-2z}}+\Upsilon(z)-\alpha\Upsilon(z-\tfrac{1}{2})+\cdots\ . \tag{B14}$$

The integral corresponding to $f(\alpha,z)$ is given by

$$\frac{1}{\pi}\int d\vec{P}\frac{e^{-\alpha P}}{P^{2z}}=\frac{2\Gamma(2-2z)}{\alpha^{2-2z}}\ ,\quad z<1\ , \tag{B15}$$

where $d\vec{P}=dn_1dn_2$, taking the P^2 for a square lattice. This equals the first term in Eq. (B14), which is singular in α about $\alpha=0$ (when $z<1$). Thus, we have

$$\lim_{\alpha\to0}\left[\sum{}'\frac{e^{-\alpha P}}{P^{2z}}-\frac{\omega}{\pi}\int\frac{e^{-\alpha P}}{P^{2z}}\,d\vec{P}\right]=\Upsilon(z)\ ,\quad z<1\ . \tag{B16}$$

Now,

$$-\ln P^2=\left[\frac{\partial}{\partial z}P^{-2z}\right]_{z=0}\ , \tag{B17}$$

so we get for b, defined in Eq. (B4),

$$b=-\tfrac{1}{2}\Upsilon'(0)\ . \tag{B18}$$

Equation (B10) can be used to yield an expression for b in terms of an infinite series. However, we also have the following forms for $\Upsilon(z)$.[15] For a square lattice,

$$\Upsilon(z)=4\pi^{-z}\zeta(z)\beta(z)\ , \tag{B19}$$

$$\beta(z)\equiv\sum_{j=0}^{\infty}(-1)^j/(2j+1)^z\ , \tag{B20}$$

and for the triangular lattice,

$$\Upsilon(z)=6(2\pi)^{-z}3^{-z/2}\zeta(z)[\zeta(z,\tfrac{1}{3})-\zeta(z,\tfrac{2}{3})]\ , \tag{B21}$$

where $\zeta(z,v)$ is the generalized zeta function. The behavior of these functions about $z=0$ is known[15]

$$\zeta(z,v)=\tfrac{1}{2}-v+z\ln\frac{\Gamma(v)}{(2\pi)^{1/2}}+O(z^2)\ , \tag{B22}$$

$$\beta(z)=\tfrac{1}{2}+z\ln\frac{\Gamma(\frac{1}{4})}{2\Gamma(\frac{3}{4})}+O(z^2)\ , \tag{B23}$$

and $\zeta(z)=\zeta(z,1)$. Using the reflection formula for the Γ function we find finally for the square lattice

$$b=\ln\{[\Gamma(\tfrac{1}{4})]^2/2\pi\}=0.738\,167\,983\cdots \tag{B24}$$

and for the triangular lattice

$$b=\ln\{[\Gamma(\tfrac{1}{3})]^3 3^{1/2}/(2\pi)^{3/2}\}=0.748\,752\,486\cdots \tag{B25}$$

The triangular lattice makes the free energy smaller so it is preferred. The latter is the value used in the text.

Stauffer and Fetter[4] also derived Eq. (8) by approximating the vortex array by a cylinder of constant vorticity of radius r_c and adding a term

$$N \ln\left[\left(\frac{\pi}{\omega}\right)^{1/2} \frac{R}{a} e^{-c/\pi}\right] , \tag{B26}$$

as the correction for a discrete lattice. This leads to Eq. (8) with the association

$$b = \frac{c}{\pi} - \frac{\ln\pi}{2} . \tag{B27}$$

For the number c, Stauffer and Fetter used the result of a calculation by Tkachenko,[16] who expressed c for any lattice in terms of θ functions. For the triangular lattice he gives $c = 4.150\cdots$. Evaluating his series we find 4.150 412 807 7, and this agrees with our result (B25) by virtue of Eq. (B27). For the square lattice Tkachenko finds $c = 4.117$ and this is consistent with Eq. (B24).

APPENDIX C

The deviation from solid-body rotation of the velocity at the vortex positions in a circular region of a triangular vortex lattice is considered here. To the extent this velocity deviation, which we call "destabilizing," is nonzero, those vortex positions are not stable and the pattern is not a local minimum of the free energy.

Let the lattice points be given by the complex numbers,

$$z(n_x,n_y) = n_x a_x + i n_y a_y , \tag{C1}$$

where $a_x = \frac{1}{2}$, $a_y = \sqrt{3}/2$, and n_x, n_y are integers, either both odd or both even. Then the distance between nearest neighbors is 1 and the density of lattice points is $2/\sqrt{3}$. For unit circulation κ, the velocity at the edge of a circular region of radius R, in the limit of large R, is $\pi R^2 (2/\sqrt{3})(1/R) = \Omega R$ which gives the angular velocity $\Omega = 2\pi/\sqrt{3}$. A "crystallographic" direction from the origin is specified by the integer pair (k_x,k_y) corresponding to lattice points

$$z(n) = n(k_x a_x + i k_y a_y) . \tag{C2}$$

The velocity $\bar{v}(n)$ at $z(n)$ in the fixed, laboratory reference frame is

$$v_x(n) - i v_y(n) = -i \sum_{\{n_x,n_y\}}^{R_0} \frac{1}{z(n) - z(n_x,n_y)} , \tag{C3}$$

where the sum is over all lattice points within a radius R_0. We consider only an unbounded system because we wish to inspect, under conditions that most favor stability, the trend of the destabilizing velocity as the pattern size increases. The radial and angular components of $v(n)$ are given by the real and negative imaginary parts, respectively, of $z(n)\bar{v}(n)/R$ where $R \equiv |z(n)|$.

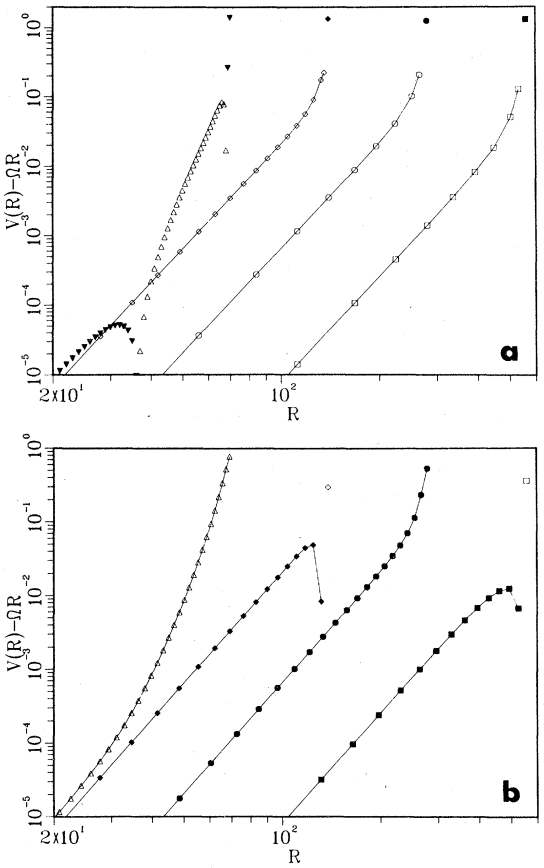

FIG. 10. Destabilizing angular velocity vs radius for patterns 1 through 4. Solid symbols denote negative velocity. The crystallographic direction is (2,0) in (a) and (3,1) in (b).

In Fig. 10 we show the relative angular velocity in directions (2,0) and (3,1) for four arrays with radii and vortex numbers listed in Table IV. Except for pattern-1 data in Fig. 10(a), velocities of equal sign

TABLE IV. Pattern radii and vortex numbers in Fig. 10. The radii are in units of the intervortex spacing.

Pattern	Radius, R_0	N
1	70	17 761
2	140	71 089
3	280	284 431
4	560	1 137 619

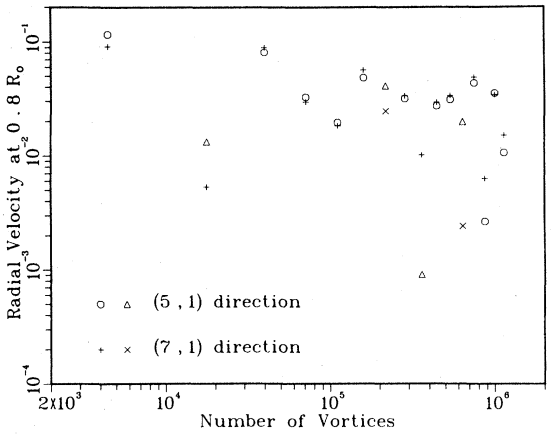

FIG. 11. Destabilizing radial velocity at a radius near 80% of the radius of the array. Triangles and crosses denote negative velocity.

are joined with straight lines. To test the radial component of the destabilizing velocity, which is zero by symmetry in the (2,0) and (3,1) directions, we calculate the velocity at one lattice point in the (5,1) and (7,1) directions for many different arrays. The radius of each point is as near as possible to 80% of the radius of the respective array. These results for the radial velocity are shown in Fig. 11. On the basis of this data we draw the following conclusions about circular regions of the triangular lattice:

(i) There is no significant tendency for the absolute destabilizing velocity at the same relative radius R/R_0 to decrease in larger arrays.

(ii) Within a circular array both the angular and radial components of the destabilizing velocity vary as $C(R/R_0)^5$, except near the edge. The constant C varies by a factor of 10 or more among different arrays but is the same, for the examples we calculated, in the (2,0) and (3,1) directions. The exponent 5 is due to the sixfold symmetry of the array. [For the square lattice the destabilizing velocity varies as $C(R/R_0)^3$.]

(iii) Arrays of many thousands of vortices still retain a strong "individuality" as illustrated in pattern 1 and by the variation in the magnitude and sign of the data in Fig. 11. Pattern 1 seems to be a transition between arrays of smaller radius, such as $R_0=69$, which have positive (2,0) destabilizing velocity and those of larger radius, such as $R_0=71$, which have negative. At $R_0=78$ the velocity is positive again. We do not know what characteristics of the patterns correlate with either this behavior or the variations in C.

(iv) The destabilizing velocity of a few lattice points near the edge of an array often has the opposite sign from the interior velocity.

Kiknadze and Mamaladze[17] have reported calculations of the velocity distribution between certain lattice points in an array identical, by our choice, to pattern 2. They also calculated, but did not list, the velocity at some lattice sites in the (2,0), (3,1), and (1,1) directions, the latter equivalent to (2,0). However, they attributed the nonzero velocity found at these lattice sites to computer round-off error and interpreted the relatively small magnitude as evidence of the accuracy of their calculation. This stems from their apparent assumption that this finite version of a triangular lattice is stable. Our round-off error was several orders of magnitude smaller than the destabilizing velocities we report. This was determined by comparing velocities calculated at equivalent lattice points and by calculating velocities known to be zero such as the radial velocity in the (2,0) and (3,1) directions. Although the general features of the intervortex velocity distribution found by the above authors for an unstable array are probably retained in a stable array, we think it is important to be aware of the limitations to this procedure.

---

*Present address: Dept. of Mechanical Engineering, SUNY, Stony Brook, N. Y. 11794.

[1]See, for example, S. J. Putterman, *Superfluid Hydrodynamics* (North-Holland, Amsterdam, 1974), especially Sec. 18.

[2]T. H. Havelock, Philos. Mag. 11, 617 (1931).

[3]G. B. Hess, Phys. Rev. 161, 189 (1967).

[4]D. Stauffer and A. L. Fetter, Phys. Rev. 168, 156 (1968).

[5]M. J. V. Gordon, G. A. Williams, and R. E. Packard, J. Phys. (Paris) 39, C6-172 (1978).

[6]See Hess, Ref. 3, and also A. L. Fetter, Phys. Rev. A 138, 429 (1965).

[7]From Eq. (5) we can derive a useful estimate for the radius r_j of a circular ring containing N_j vortices in a pattern of $N=\sum_1^N N_j$ vortices in M ordered rings

$$\omega r_j^2=\tfrac{1}{2}(N_j-1)+\sum_1^{j-1}N_i \ .$$

In particular, the radius of the pattern is, to good approximation,

$$r_M^2=(2N-N_M-1)/2\omega \ .$$

Including images would increase the size of the pattern because the images effectively attract the vortices.

[8]See H. Lamb, *Hydrodynamics*, 6th ed. (Dover, New York, 1945), p. 230.

[9]L. J. Campbell and R. M. Ziff, Los Alamos Scientific Laboratory Report No. LA-7384-MS, 1978 (unpublished). Copies are available from the authors upon request.

[10]Solutions for N exist only if $\omega_1\leq\omega\leq\omega_2$ where

$$\omega_1+\tfrac{1}{2}\ln\omega_1=\ln(R/a)-b$$

and

$$\omega_2=(R/a)^2e^{-2b} \ .$$

Note that solid-body rotation corresponds to $N\kappa = 2\pi R^2 \Omega$ or $N = \omega$. For this to be compatible with Eq. (10) requires that $\omega = \omega_2$ which then yields the classical results for the free energy from Eq. (8),

$$f_c(N = \omega, \omega = \omega_2) = -\frac{1}{4}\omega^2|_{\omega=\omega_2} .$$

[11]L. J. Campbell and R. M. Ziff, J. Phys. (Paris) 39, C6-222 (1978).

[12]R. E. Packard and T. M. Sanders, Phys. Rev. Lett. 22, 823 (1969).

[13]R. M. Ziff, G. E. Uhlenbeck, and M. Kac, Phys. Rep. C 32, 169 (1977).

[14]E. T. Whittaker and G. N. Watson, *Course of Modern Analysis* (Cambridge University, Cambridge, England, 1927).

[15]A. Erdetyi *et al.*, *Higher Transcendental Functions* (McGraw-Hill, New York, 1953), Secs. 1.10–1.12. For the properties of $\beta(z)$ see M. L. Glasser, J. Math Phys. 14, 409 (1973), Appendix. Note that his $\beta'(0)$ is incorrect by a factor of 2.

[16]V. K. Tkachenko, Sov. Phys. JETP 22, 1282 (1966).

[17]L. V. Kiknadze and Yu. G. Mamaladze, Sov. J. Low Temp. Phys. 2, 731 (1976).

[18]E. J. Yarmchuk, M. J. V. Gordon, and R. E. Packard, Phys. Rev. Lett. 43, 214 (1979).